Liquid Crystals
Publication details, including instructions for authors and subscription information:
http://www.informaworld.com/smpp/title~content=t713926090

The phase behaviour and optical properties of a nematic/chiral dopant liquid crystalline mixture system

Wen-Ren Chen[a]; Jenn-Chiu Hwang[a]
[a] Department of Chemical Engineering and Materials Science Yuan-Ze University Neili, Taoyuan Taiwan 320 ROC,

Online publication date: 11 November 2010

To cite this Article Chen, Wen-Ren and Hwang, Jenn-Chiu(2004) 'The phase behaviour and optical properties of a nematic/chiral dopant liquid crystalline mixture system', Liquid Crystals, 31: 11, 1539 — 1546
To link to this Article: DOI: 10.1080/02678290412331304113
URL: http://dx.doi.org/10.1080/02678290412331304113

LIQUID CRYSTALS, 2004, VOL. 31, NO. 11, 1539–1546

Taylor & Francis
Taylor & Francis Group

The phase behaviour and optical properties of a nematic/chiral dopant liquid crystalline mixture system

WEN-REN CHEN and JENN-CHIU HWANG*

Department of Chemical Engineering and Materials Science,
Yuan-Ze University, Neili, Taoyuan, Taiwan 320, ROC

(*Received 28 April 2004; accepted 25 July 2004*)

The phase behaviour and aggregation states of a binary mixture of a nematic liquid crystal and a chiral dopant have been investigated. The nematic liquid crystal E7 was miscible with the chiral dopant S811 over their entire concentration range. Binary E7/S811 mixtures formed the N* phase for S811 contents under 20%, and the SmA* phase for S811 contents between 40% and 90%. BP and TGBA* frustrated phases were found during cooling, for S811 contents between 25% and 35%. The helical pitches of the binary mixtures decreased with increasing chiral dopant content. From XRD profiles, the orientational ordering of the binary composites was found to increase with increasing chiral dopant content.

1. Introduction

The blue phase (BP) and twist grain boundary (TGB) phase are two frustrated liquid crystalline phases found originally discovered in 1888 [1] and 1989 [2], respectively. The former has a characteristic the brilliant platelet texture and appears between the isotropic liquid and chiral nematic phase. It was not recognized as a new thermodynamically stable phase until the mid 1970s. This blue phase has been subdivided into three sub-phases, the BPI, BPII and BPIII phases, according to chirality and the phase transition temperature [3–7]. BPI and BPII are modelled as body-centered cubic and simple-cubic structures, respectively. However, BPIII is thought to have an amorphous state and is named 'blue fog'. The blue phases are often found in a narrow temperature range of about 1°C. Recently, Hirotsugu *et al*. reported several polymer/BP composites that preserve the blue phase at temperatures above 60°C [8].

The TGB phase exhibits a filament texture and is normally observed between the chiral nematic (N*) and smectic A (SmA) or smectic C (SmC) phases. Many homologous series of ferroelectric or cholesteric liquid crystals with high chirality have been reported to exhibit the TGB phase [2, 9–14]. The TGB phase has also appeared in some mixtures of two or more liquid crystalline materials [7, 15–18]. Renn and Lubensky were the first to predict the existence of the TGB phase between the N* and smectic phases [19]. The proposed TGB structure is characterized by a helical superstructure and smectic layer, with the helical axis parallel to the smectic layer plane [16].

Earlier reports concerned the frustrated liquid crystalline phase of single [9–14] or multi-component mixtures including cholesteric or ferroelectric liquid crystals with high chirality [15–18]. Dierking described a mixture consisting of a ferroelectric compound (D8) with a chiral dopant (C4) possessing the BP and TGB phases [16]. Dhar *et al*. studied a mixture of a cholesteric compound (5-cholesten-3g-ol-octanoate) and a nematic compound (4-*n*-nonyloxybenzoic acid) which induced the BP and TGB phases [18]. We have also mixed two nematic liquid crystals and a cholesteric liquid crystal to induce the BP and TGB phases [7]. However few studies have sofar been made on systems comprising a nematic mesogen and a non-liquid crystalline chiral dopant.

In this paper, therefore, we report experiments on mixtures of the nematic liquid crystal E7 with a chiral dopant S811 (which has no liquid crystalline phases), and discuss the induced liquid crystalline mesophases. The phase behaviour and transition temperatures of E7/S811 mixtures of varying composition are reported. The helical pitches and orientational ordering in the binary mixtures were also investigated.

2. Experimental

Figure 1 shows the chemical structures of materials used in the experiments. Both E7 (nematic liquid crystal) and S811 (chiral dopant) were bought from Merck Ltd., Japan and used without further purification.

*Author for correspondence;
e-mail: cejhwang@saturn.yzu.edu.tw

Liquid Crystals ISSN 0267-8292 print/ISSN 1366-5855 online © 2004 Taylor & Francis Ltd
http://www.tandf.co.uk/journals
DOI: 10.1080/02678290412331304113

(1) Nematic liquid crystal : E7

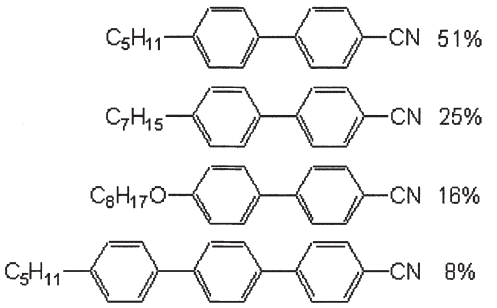

Cr - -10℃ - N - 60℃ - I

(2) Chiral dopant : S811

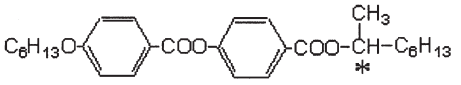

Cr - 47.8℃ - I

Figure 1. The chemical structures of the nematic liquid E7 and chiral dopant S811.

The nematic liquid crystal/chiral dopant mixture was first dissolved in a solvent (acetone) and a composite was prepared by evaporating the solvent. The composites were sandwiched between two transparent ITO glass substrates separated by 12 μm PET spacers. In this study, the ITO glass surfaces were not coated by an alignment layer, but were treated by rubbing in afterwards; therefore, the orientation of the composite molecules was random.

Helical pitches of the binary composite were measured by the Grandjean–Cano method [20]. Spacers inserted between a pair of glass substrates with different rubbing directions: 100 μm for a helical pitch longer than 2 μm; 25 μm for a helical pitch shorter than 2 μm.

The phase transition behaviour and aggregation states of the E7/S811 composite were investigated by differential scanning calorimetry (DSC, Perkin-Elmer DSC-7) and polarizing optical microscopy (POM, Nikon FXA equipped with a hot stage, Mettler FP82 and FP90). The DSC scanning rate was 0.2 and 3°C min^{-1}. The cooling rate was 0.1–3°C min^{-1} during the POM observation of phase transition.

The mesophase was confirmed by X-ray powder diffraction (XRD) conducted at the BL17A1 beamline of the National Synchrotron Radiation Research Center (NSRRC). Samples were sealed in a 1 mm capillary on the Huber 5020 four-circle diffractometer for the transmission type XRD used. The low angle diffraction was collected using a step scan of 0.02° for 2θ ranging from 1° to 10° at the wavelength 1.33295 Å. The scanning step was 0.05° for the 2θ range 10° to 25°. The cell temperature was elevated and lowered with a stream of computer-controlled hot or ambient air.

3. Results and discussion

3.1. *Phase behaviour and aggregation states of the binary composites*

The nematic liquid crystal E7 was miscible with the chiral dopant S811 over their entire concentration range. Many mesophases were induced in the various E7/S811 weight fractions. Figure 2 shows optical photomicrographs of the E7/S811 composites 98/2 and 80/20. As shown in figure 2 (*a*), the fingerprint texture was observed in the 98/2 mixture. The same textures were observed in the composition range 99.5/0.5–95/5, but the widths between two adjacent stripe lines in these textures became shorter with increasing S811 content. Figure 2 (*b*) shows focal-conic texture in the 80/20 sample. The fingerprint and focal-conic textures were observed in the S811 content ranges of 0.5–5 and 5–20%, respectively. Both the fingerprint and

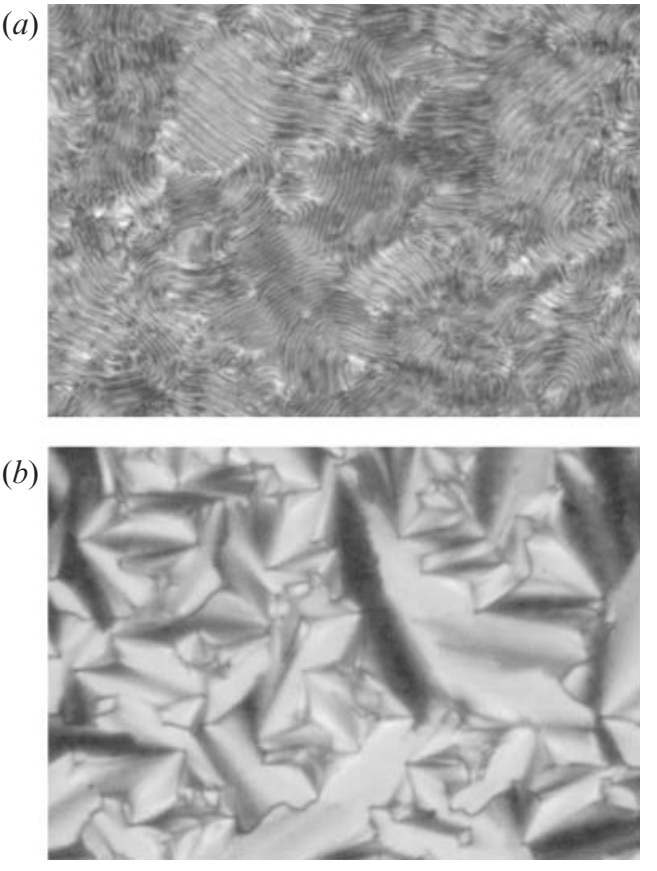

Figure 2. The photomicrographs of (*a*) the 98/2 and (*b*) the 80/20 composites in the N* phase (T=37 and 38.8°C, respectively).

focal-conic textures were one of the optical textures seen in the N* phase. The N* was the only phase found for the binary composite in the range 99.5/0.5–80/20.

It was of interest to study the phase behaviour in the composition range 75/25–65/35. Figure 3 shows photomicrographs of the 70/30 sample during slow cooling ($0.2^{\circ}C\,min^{-1}$) from the isotropic liquid (I). A grey platelet texture with dark background (BPII) was observed in the 70/30 composite at 38.5°C, as shown in figure 3 (*a*). This gradually formed a typical BPII phase with colourful platelets [21]. On further cooling, the BPI (*b*), N* (*c*), TGBA* (*d*) and SmA* (*e*) phases were observed. The same phase sequence, with different transition temperatures, was found in the 75/25 composite. When cooling the 65/35 mixture, the blue phase changed directly to the SmA* phase and no TGB phase was observed. It was surprising that the SmA* phase with fan-shaped texture was induced in the composition range 60/40–10/90. When the S811 content became higher than 90%, the induced SmA* phase was replaced by needle-like crystals.

Figure 4 is a thermal analysis diagram for binary E7/

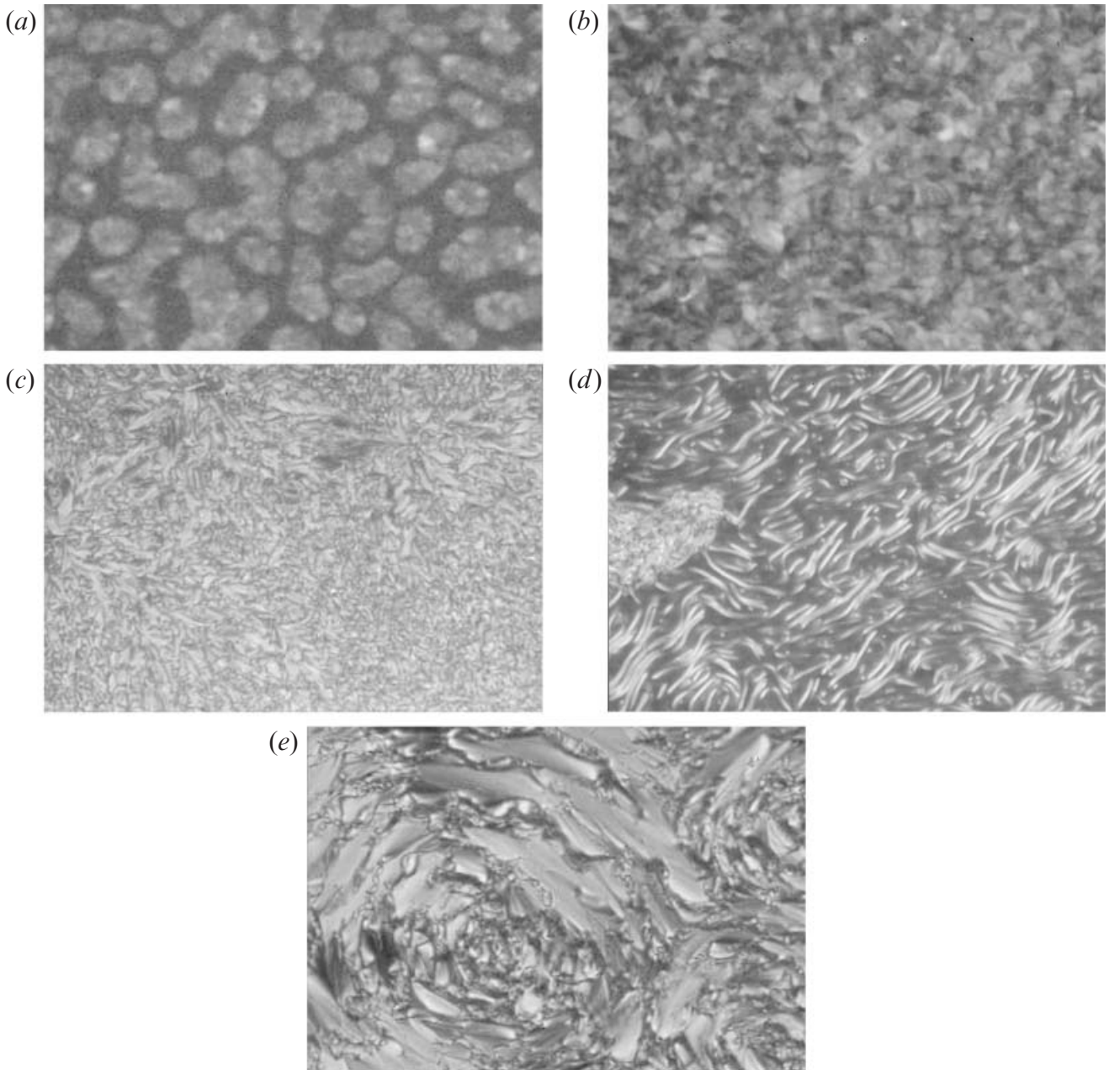

Figure 3. Photomicrographs of the 70/30 composite: (*a*) BPII phase, $T=38.5^{\circ}C$, (*b*) BPI phase, $T=37^{\circ}C$, (*c*) N* phase, $T=32.7^{\circ}C$, (*d*) TGBA* phase, $T=24.6^{\circ}C$ and (*e*) SmA* phase, $T=23^{\circ}C$.

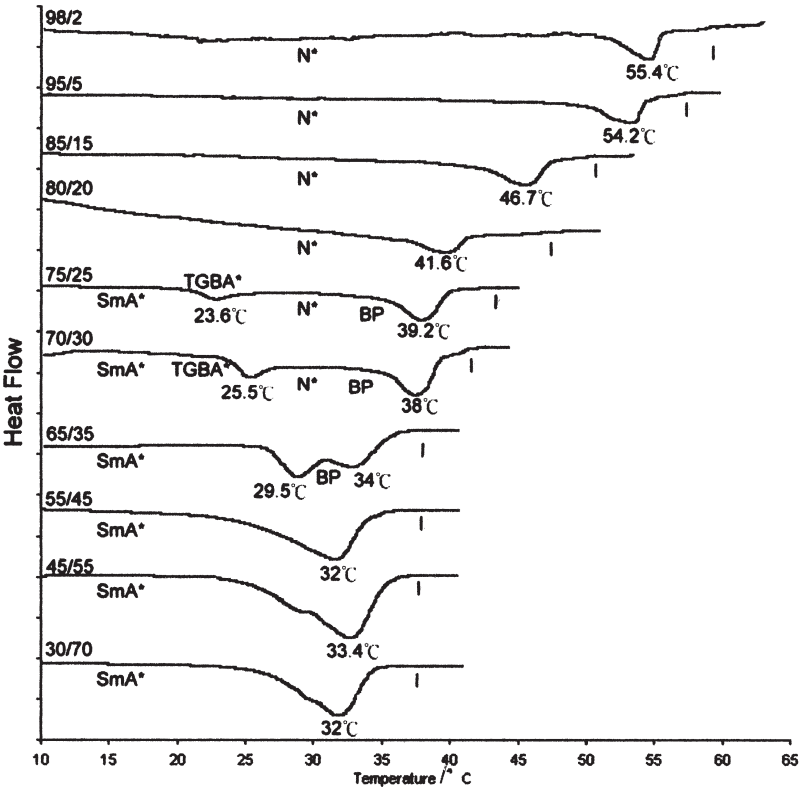

Figure 4. DSC diagram for E7/S811 composites measured at $3^{\circ}C\,min^{-1}$ scanning rate in 98/2 to 30/70 mixing ratio.

S811 composites of different weight ratios. The DSC curves were derived during the second cooling process, at a rate of $3^{\circ}C\,min^{-1}$. Only one phase transition peak was observed for S811 $<20\%$, and corresponded to the I–N* phase transition. The phase transition temperature decreased with increasing S811 weight fraction. As the S811 content increased to 25 and 30%, two phase transition peaks were found; however, six mesophases (I,BPII,BPI,N*,TGBA*,SmA*) formed during cooling under POM, perhaps some phase transition peaks were too small for observation. On increasing the S811 content to 35%, the N* phase disappeared; two phase transition peaks were observed, corresponding to the I–BP and BP–SmA* transitions. A broad and diffuse peak was observed for S811 content over 40%, indicating the I–induced SmA* phase transition. No liquid crystalline mesophase was found in the S811 content range 90–100%.

In order to find the BP–N* and N*–TGBA* phase transition peaks in the 75/25 and 70/30 mixtures, a further thermal analysis was carried out with a cooling rate $0.2^{\circ}C\,min^{-1}$, see figure 5. Five peaks were observed during this cooling scan; corresponding to I–BPII, BPII–BPI, BPI–N*, N*–TGBA* and TGBA*–SmA* phase transitions. It was noted that the BPII phase was observed in a very narrow temperature range (0.8°C) between the isotropic liquid and the BPI phase. Nevertheless, the temperature range of the BPI phase was about 4.8°C. The enthalpy changes were all under $0.5\,J\,g^{-1}$, the smallest being $0.089\,J\,g^{-1}$ for the BPI–N* transition. The same phase sequence was found in the 75/25 mixture.

Table 1 summarizes the liquid crystalline mesophases, phase transition temperatures and enthalpy changes of the E7/S811 composite. The enthalpy changes of the I–N* phase transition were $0.64–1.26\,J\,g^{-1}$ with the S811 content $<20\%$, and $5.46–8.87\,J\,g^{-1}$ for the I–SmA* transition with the S811 content $>45\%$. No relationship between the enthalpy change and S811 content was obvious for the I–N* phase transition. However, for the I–SmA* transition, the enthalpy change increases with increasing S811 content. The orientational ordering increases with increasing S811 content, and more energy must be released when the SmA* phase is formed.

Figure 6 shows the eutectic phase diagram for the binary E7/S811 composite. All the phase transition temperatures of the composites were verified by DSC. From this phase diagram, it can be seen that the phase sequence of the 65/35 sample is I–BP–SmA*. The optical texture of this blue phase is a monodomain with blue colour; it may be categorized as blue fog (BPIII).

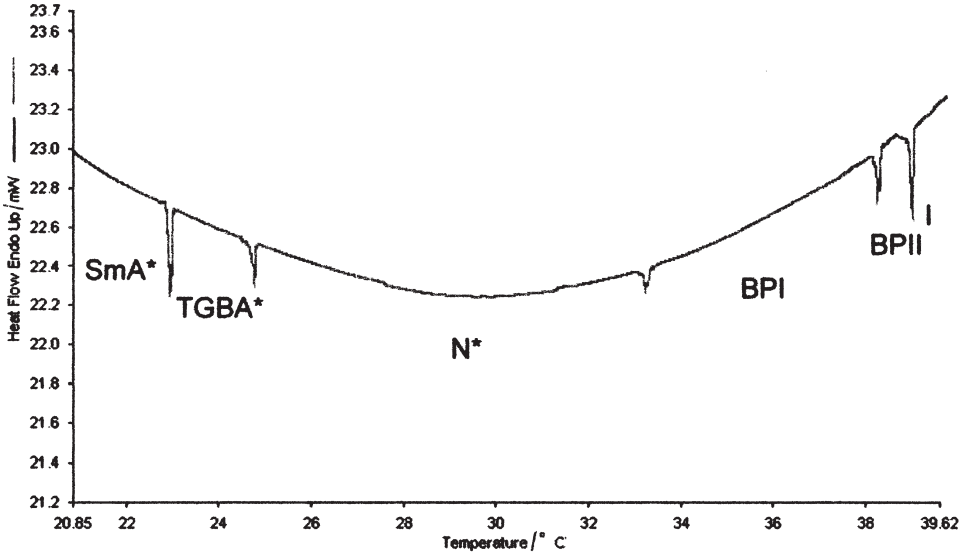

Figure 5. DSC diagram for the 70/30 composite cooling at 0.2°C min^{-1}.

The temperature range of the blue phase in these mixtures exceeded 1°C.

3.2. *Helical pitch measurements*

To examine the effect of the chiral dopant, the Grandjean–Cano method was used to measure the helical pitches of binary composites. Photomicrographs of the Cano cell under POM observation were taken at room temperature (25°C, N* phase). We tried to observe the Grandjean lines during cooling, but only disordered oily streak textures were seen. However, after uniformly pressing the Cano cell, Grandjean steps were found under POM observation. The distances between adjacent Garndjean lines were measured with the help of objective microscope micrometer (100 scales within 1 mm), and the helical pitches were calculated for E7/S811 compositions ranging from 99.5/0.5 to 70/30. Figure 7 shows the dependence of helical pitch and twist angle of the binary composites on the S811 weight fraction of (twist angle is 360°/helical pitch P). It can be seen that the pitch was about 8.8 μm for an S811 content of 0.5%; on adding more S811 (0.5–5%), the

Table. The liquid crystalline mesophases, phase transition temperatures (°C) and enthalpy changes (J g^{-1}, in brackets) of E7/S811 composites of different weight fractions. I = isotropic, N = nematic, N* = chiral nematic, BP = blue phase, TGB = twisted grain boundary phase, Sm = Smectic, Cr = crystal.

Concentration/%		
E7	S811	Phases
100	0	I 56.23(2.55) N
99.5	0.5	I 56.67(1.13) N*
98	2	I 55.40(1.26) N*
95	5	I 54.23(0.64) N*
85	15	I 46.73(0.72) N*
80	20	I 41.60(1.45) N*
		I 39.80(0.39) BPII 38.93(0.27)
		BPI 33.79(0.07) N* 23.86(0.23)
75	25	TGB 22.69(0.43) SmA*
		I 38.96(0.26) BPII 38.16(0.16)
		BPI 33.40(0.09) N* 24.72(0.13)
70	30	TGB 22.93(0.30) SmA*
65	35	I 34.0(1.01) BP 29.5 (1.18) SmA*
55	45	I 31.98(5.46) SmA*
45	55	I 33.40(6.91) SmA*
30	70	I 31.98(8.87) SmA*
10	90	Cr 42.68 (62.68) I & I 25.56(10.55) Cr
0	100	Cr 48.10 (77.42) I & I 32.23(80.54) Cr

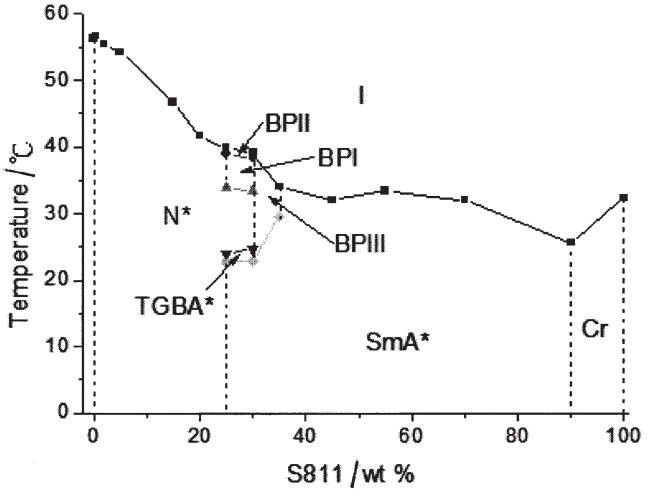

Figure 6. E7/S811 phase diagram.

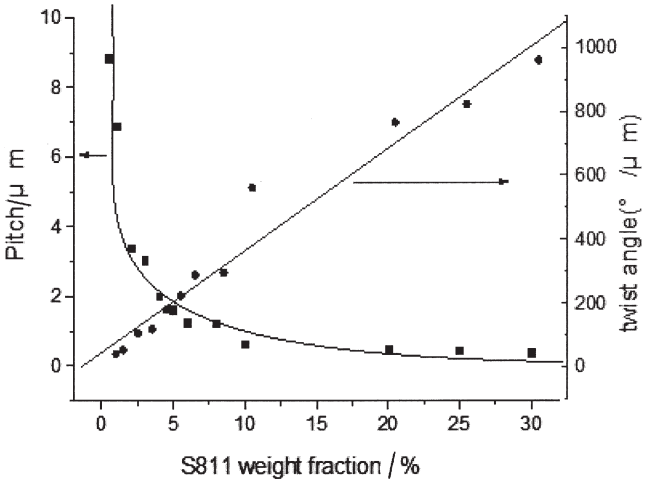

Figure 7. Helical pitch and twist angle (360°C/helical pitch) measured for different E7/S811 composites.

helical pitch quickly dropped to 1.6 μm, then slowly decreased to 0.38 μm (5–25%). The twist angle of the composite was directly proportional to the S811 content; thus the twist angle of two adjacent molecules in the composite increases with increasing the chiral dopant content.

Figure 8 shows the effect of different rubbing directions of the glass substrates in the Cano cell. Grandjean steps were influenced by the alignment at the surface of the glass substrate, a rubbing direction parallel to the long or narrow sides of the cell inducing ordered steps, figures 8 (*a*) and 8 (*b*). However, disordered oily streak textures were observed after inclined or anti-parallel rubbing, figures 8 (*c*) and 8 (*d*).

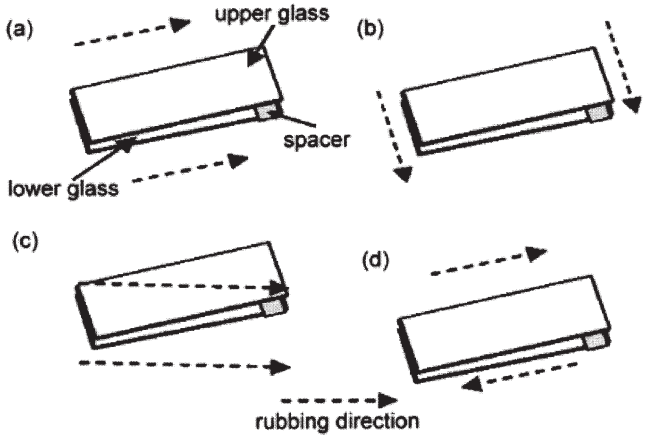

Figure 8. The effect of different rubbing directions of the Cano cell on the formation of Grandjean textures. Parallel to the long (*a*) and narrow (*b*) sides of the cell are better for full alignment. Anti-parallel to long side (*c*) and inclined rubbing (*d*) results in a randomly oriented planar texture.

3.3. *X-ray diffraction*

Figure 9 shows XRD profiles of binary composites of composition 80/20, 75/25, 65/35 and 30/70, at a temperature of 28°C. A diffuse reflection peak corresponding to the intermolecular distance was observed at the wide Bragg angle for all samples. Another weak and diffuse peak was found at low or mid 2θ angle in the 80/20 sample (N* phase); this was an appropriate result in the N* phase for a liquid crystalline system. The maximum normalized intensity was found around $2\theta = 2.7°–2.9°$. The corresponding *d*-spacing was calculated to be 26–28 Å, close to the molecular length of E7 and S811. This peak, at low 2θ angle, became sharper and stronger in the 75/25 sample, with maximum normalized intensity at 2.74° and *d*-spacing 27.88 Å. The mesophase of this sample was also N* (28°C) but the molecular orientation seems more ordered than the former. The maximum normalized intensity of the peak at low 2θ rose quickly in the 65/35 and 30/70 samples. The mesophase of these two samples was smectic by POM, which was confirmed by XRD. In summary, the low angle peak was weak and diffuse in composites with low S811 concentration, and became stronger and sharper with increasing S811 content. It is supposed that the molecular orientation in the binary composite becomes more ordered as the content of chiral dopant increases.

Figure 10 shows XRD profiles of the E7/S811 = 70/30 composite during cooling. The shape and intensity of the peak in the BPII phase was diffuse and weak at low angle (about $2\theta = 2.5–3.0°$); it became sharper and stronger with decreasing temperature. The BPI phase appeared to have a smectic order and might be a smectic blue phase [11, 22]. The orientational ordering

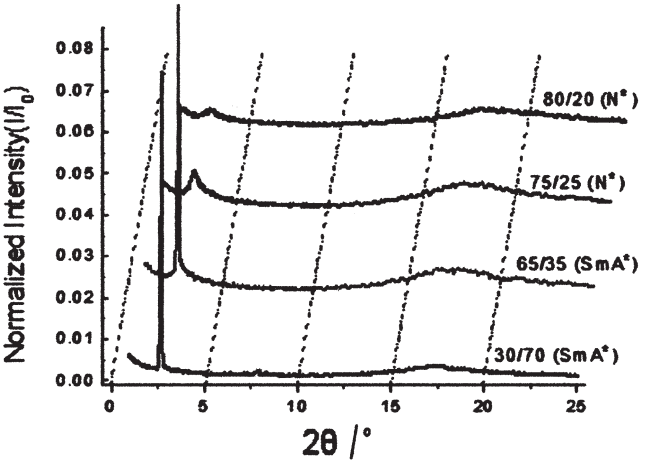

Figure 9. XRD profile of the 80/20, 75/25, 65/35 and 30/70 composites measured at 28°C.

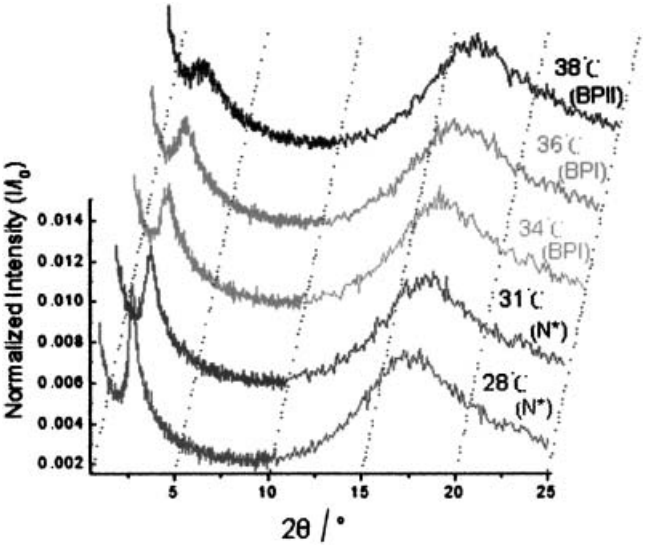

Figure 10. XRD profiles of the 75/25 composite at different temperatures.

changed from a disordered BP phase to the more ordered SmA* phase with decreasing temperature.

In order to identify the smectic phase in the 55/45–20/80 samples, further XRD analyses were performed at different temperatures. Figure 11 gives the XRD profiles for the 20/80 composite at 34, 31 and 28°C. A diffuse peak corresponding to the intermolecular distance was observed around 15–20° in the three samples. A sharp peak was seen at 2.7°, its maximum normalized intensity increasing with decreasing the temperature. The corresponding layer spacing did not fall with decreasing the temperature. Thus, we conclude that this induced smectic phase is the SmA* phase. The same results were observed for the 55/45 and 30/70 mixtures.

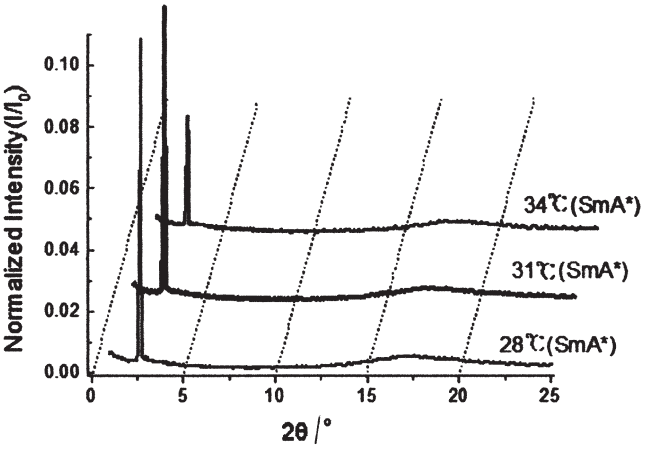

Figure 11. XRD profile of the 20/80 composite at different temperatures.

We propose a possible orientation and stacking structure as shown in figure 12. The chiral dopant S811 has rod-like molecules, with a molecular length close to that of the NLC E7 molecules. The chiral dopant could thus align with the nematic liquid crystal. When the chiral dopant content is small, the weaker helical power of the NLC drives its molecules to orient in a helical fashion, with the axis parallel to the substrate glass, thus developing the N* phase as shown in figure 12 (*a*). With this low level of chiral dopant, every chiral molecule drives the neighbouring nematic molecules to rotate by only a small angle, which results in long helical pitches. On adding more chiral dopant, the helical power rises and the twist angle of the adjacent molecules becomes higher. As shown in figure 12 (*b*), fewer molecules are involved in a 2π helical period and the helical pitch decreases. This is still the N* phase but the optical texture changes to focal–conic under POM observation. If the chiral dopant content is above a threshold value (40% here), the positional and orientational ordering may increase to give a SmA* phase more ordered than the N* phase, as shown in figure 12 (*c*). The mixture would then lose the twist deformation and helical pitches. This explains the formation of N* and SmA* phases at lower and higher S811 concentrations, respectively.

4. Conclusions

We report that a nematic liquid crystal E7 is miscible with a chiral dopant S811 over their entire concentration range. The binary E7/S811 mixture formed the N* or SmA* phase with the S811 content below 20% or in the range 40–90%, respectively. Frustrated BP and TGBA* phases were found in the 25–35% S811 content range during cooling. The helical pitche of binary mixtures in the N* phase was measured by the

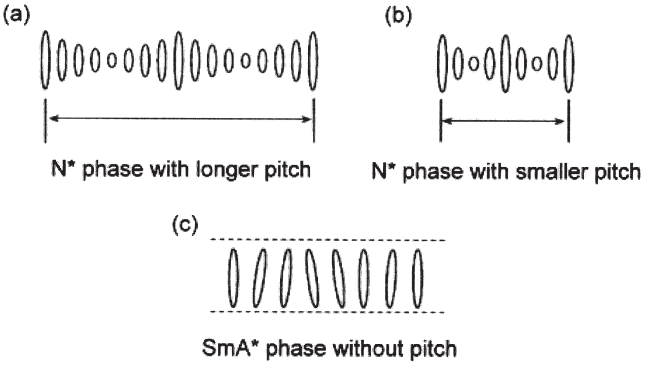

Figure 12. Schematic illustrations of molecular orientation in binary composites of different S811 weight fraction. (*a*) The N* phase with longer helical pitch, (*b*) the N* phase with smaller helical pitch and (*c*) the SmA* phase without helical pitch.

Grandjean–Cano method; it decreased with increasing S811 concentration. From the XRD profiles, we found that the orientational ordering of the binary composites increased with increasing chiral dopant content. The mesophases transformed from N* to SmA* with increasing chiral dopant content.

References

[1] Reinitzer, F., 1888, *Monatsh. Chemie*, **9,** 421.
[2] Goodby, J. W., Waugh, M. A., Stein, S. M., Chin, E., Pindak, R., and Patel, J. S., 1989, *Nature*, **337,** 449.
[3] Meiboom, S., and Sammon, M., 1980, *Phys. Rev. Lett.*, **44,** 882.
[4] Meiboom, S., Sethna, J. P., Anderson, P. W., and Brinkman, W. F., 1981, *Phys. Rev. Lett.*, **46,** 1216.
[5] Yang, D. K., and Crooker, P. P., 1981, *Phys. Rev. A*, **35,** 419.
[6] Heppke, G., Kitzerow, H. S., Lötzsch, D., and Papenfuß, CH., 1990, *Liq. Cryst.*, **8,** 407.
[7] Hwang, J. C., Liang, S. C., and Liang, K. H., 1998, *Jpn. J. appl. Phys.*, **37,** 4444.
[8] Hirotsugu, K., Yokota, M., Hisakado, Y., Yang, H., and Kajiyama, T., 2002, *Nat. Mater.*, **1,** 64.
[9] Goodby, J. W., Waugh, M. A., Stein, S. M., Chin, E., Pindak, R., and Patel, J. S., 1989, *J. Am. chem. Soc.*, **111,** 8119.
[10] Dierking, I., Gießelmann, F., and Zugenmaier, P., 1994, *Liq. Cryst.*, **17,** 17.
[11] Li, M. H., Laux, V., Nguyen, H. T., Sigaud, G., Barois, P., and Isaert, N., 1997, *Liq. Cryst.*, **23,** 389.
[12] Wu, S. L., Yen, P. C., and Hsieh, W. J., 1998, *Liq. Cryst.*, **24,** 741.
[13] Bayón, R., Coco, S., and Espinet, P., 2002, *Chem. Mater.*, **14,** 3515.
[14] Cha, S. W., Jin, J. I., Achard, M. F., and Hardouin, F., 2002, *Liq. Cryst.*, **29,** 755.
[15] Booth, C. J., Goodby, J. W., Hardy, J. P., and Toyne, K. J., 1994, *Liq. Cryst.*, **16,** 43.
[16] Dierking, I., 2001, *Liq. Cryst.*, **28,** 165.
[17] Zhang, F., and Yang, D. K., 2002, *Liq. Cryst.*, **29,** 1497.
[18] Dhar, R., Pandey, M. B., and Agrawal, V. K., 2003, *Phase Trans.*, **76,** 763.
[19] Renn, S. R., and Lubensky, T. C., 1988, *Phys. Rev. A*, **38,** 2132.
[20] Cano, R., 1968, *Bull. Soc. Fr. Mineral. Cristallogr.*, **91,** 20.
[21] Li, M. H., Nguyen, H. T., and Sigaud, G., 1996, *Liq. Cryst.*, **20,** 361.
[22] Pansu, B., Li, M. H., and Nguyen, H. T., 1997, *J. Phys. II*, **7,** 751.